Electrical Modelling and Mismatch Effects of Thermoelectric Modules on Performance of a Thermoelectric Generator for Energy Recovery in Diesel Exhaust Systems

Samir Ezzitouni [1], Pablo Fernández-Yáñez [1], Luis Sánchez Rodríguez [1], Octavio Armas [1,*], Javier de las Morenas [2], Eduard Massaguer [3] and Albert Massaguer [3]

1   Escuela de Ingeniería Industrial y Aeroespacial de Toledo, Campus de Excelencia Internacional en Energía y Medioambiente, Universidad de Castilla-La Mancha, 45071 Toledo, Spain; samir.ezzitouni@uclm.es (S.E.); pablo.fernandezyanez@uclm.es (P.F.-Y.); luis.sanchez@uclm.es (L.S.R.)
2   Escuela de Ingeniería Minera e Industrial de Almadén (AutoLog), Campus de Excelencia Internacional en Energía y Medioambiente, Universidad de Castilla-La Mancha, 13400 Almadén, Spain; javier.delasmorenas@uclm.es
3   Department of Mechanical Engineering and Industrial Construction, University of Girona, 17003 Girona, Spain; eduard.massaguer@udg.edu (E.M.); albert.massaguer@udg.edu (A.M.)
*   Correspondence: octavio.armas@uclm.es; Tel.: +34-926-295462

Abstract: Thermoelectric generators harvesting energy from exhaust gases usually present a temperature mismatch between modules, due to the gradual cooling of the gases along the flow direction. The way modules that produce unequal voltages are connected has a deep impact on the overall power output. A further step in the prediction of thermoelectric production is to consider the complete layout of the thermoelectric modules and not consider them as isolated systems. In this work, a model to predict the electric behavior of thermoelectric generators for automotive applications at different points of operation is presented. The model allows testing of serial-parallel connection configurations. The results present good agreement with experimental data. This model could be used on similar light duty vehicles with similar engines as the engine used in this work and using similar configuration of thermoelectric generators. Simulated scenarios considering realistic operating conditions in a light duty vehicle allow stating that thermoelectric modules interconnection under heterogenous thermal surface conditions has a significant negative effect (more than 17%) on electric energy production. Moreover, the proposed model shows the need to protect the electric circuit of the thermoelectric generator to avoid the negative effect of possible malfunction of some thermoelectric modules.

Keywords: thermoelectric generator; thermal mismatch; thermal waste energy

1. Introduction

The energy balance of a reciprocating internal combustion engine shows that approximately the third part of the fuel energy intake is wasted as heat through the exhaust gases [1–3]. Nevertheless, the current trend in new developments is to make engines more adiabatic, increasing the indicated work and the exhaust flow enthalpy [4,5].

The increase in exhaust enthalpy allows to increase the efficiency of after-treatment devices [6], and thermal energy recovery for electrical energy production [7–9]. The former leads to less pollutant engines, while the latter leads to higher engine efficiency. Several alternatives are available to recover waste thermal energy [10–16], thermoelectric generators being one of the currently developing technologies.

A thermoelectric module (TEM) is a device composed of n- and p-type semiconductors that convert a temperature gradient across them in an electric voltage through the Seebeck effect. The integration of several thermoelectric modules is commonly referred to as thermoelectric generator (TEG).

The electric load connected to the TEG determines the power extracted. For fixed electric connections among TEMs, the maximum power point tracking (MPPT) method consists in adjusting the external electric load to maximize the power output.

For automotive applications, TEGs are usually placed in the exhaust system using the exhaust gas as heat source and external air or cooling water as heat sink. As the exhaust gas flows through the TEG, its temperature is decreased. This implies that TEMs within a TEG work under different hot-side temperatures depending on their location, with the subsequent electric mismatch of TEMs connected in the same electric branch.

Mori et al. [17] affirmed that the incorporation of the TEG to the exhaust system of a vehicle allows obtaining a fuel saving of 3%, but in their simulations, only electrically isolated thermoelectric modules were considered, which produces an estimation error. This occurs with most of the models designed to predict the energy generated by a TEG [18–21].

Another aspect of thermal and electric models that quantify TEG performance is that thermal mismatch of TEMs in the same electrical branch is not considered [22–25]. Kumar et al. [24] and Hsiao et al. [25] used models that predict TEG behaviour to investigate the efficiency of the heat exchangers, and to find the best location of the TEG in a light duty vehicle, respectively, but in both models, authors did not consider the possible negative effect of electrically connection of the thermoelectric modules under heterogeneous thermal conditions. This significantly reduces the accuracy of such models.

Some recent works have managed to reduce this trend [26–30], but these have not been validated under realistic working temperatures inherent to a TEG working for a light-duty vehicle. Cózar et al. [29] stated that there is an optimum number of TEMs from which an increase of the number of TEMs diminishes the power output. Montecucco et al. [30] proved, using three TEMs, that the loss in power output due to the thermal mismatch of the modules could be up to the 13%, but the test conditions were not representative of automotive operation.

Most electrical models and electrical mismatch analyses are tested under arbitrary working conditions. Taking a further step, in this work, the influence of electrical mismatch in a TEG working under realistic automotive operation conditions is presented. The TEG is installed in a light-duty diesel engine working in the most used part of its engine map during urban an extra-urban driving.

The approach followed comprises a CFD (Computational Fluid Dynamics) model to feed surface temperatures from exhaust flow inlet conditions coupled with an electric model. Once validated, the influence in power output of the different scenarios was studied: (i) thermal mismatch in TEMs in the same electrical branch, (ii) malfunction of TEMs, and (iii) variation in the number of TEMs in a branch.

This work provides an insight into the electrical operation of TEGs under realistic operation temperatures for out-of-design conditions and could help in the design process for new prototypes.

2. TEG Modelling

The computational approach is based on two stages: the first is a CFD model that calculates the three-dimensional heat transfer from the exhaust gases to the thermoelectric modules and the second models the electric performance of the interconnected modules (see Figure 1).
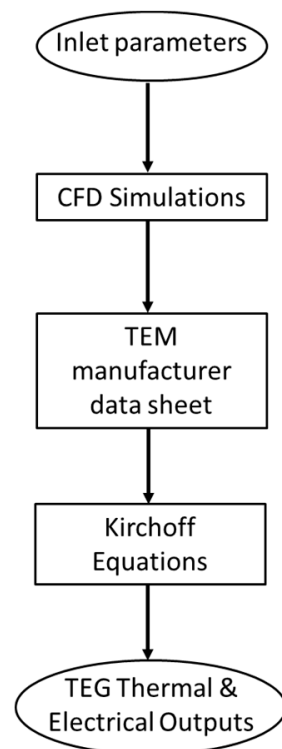
Figure 1. General view of the thermoelectric model block diagram.

2.1. CFD Model

The first part of the model consists of a three-dimensional CFD model. The simulation includes all the parts involved in the heat transfer process to the modules: the exhaust gas, the hot-side heat exchanger, the thermoelectric modules, and the cooling circuit (see Figure 2). From these simulations, a surface temperature distribution in the hot and the cold sides (see Figure 3) are obtained and fed to the second part of the model. More information about the equations solved and the numerical schemes in this part of the model can be found in Fernández-Yañez et al.'s report [31].
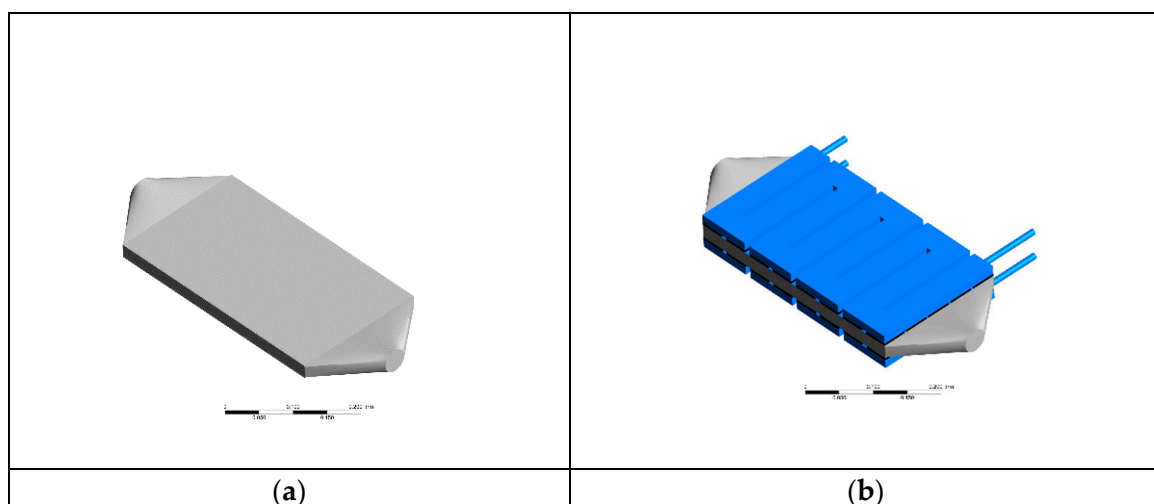

Figure 2. CFD simulation domain: (**a**) gas-side heat exchanger and (**b**) the whole TEG system.
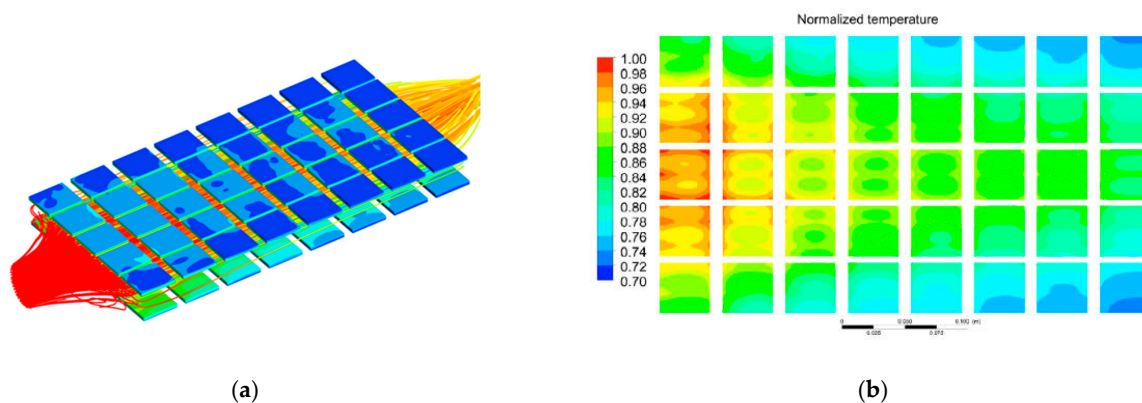
(**a**)

(**b**)

Figure 3. (**a**) 3-D reconstruction of the internal flow and the thermoelectric modules and (**b**) normalized temperature in upper-surface modules.

2.2. Electrical Model

2.2.1. Determination of Electrical Parameters

The electrical model needs a characterization of the thermoelectric modules in terms of open circuit voltage (V_{oc}) and internal resistance (R_{int}). From the information provided by the manufacturer (Figure 4), second order polynomial relationships with hot side temperature (T_h) were obtained for both parameters (Equations (1) and (2)).

$$V_{oc} = a_1 T_h^2 + a_2 T_h + a_3 \tag{1}$$

$$R_{int} = b_1 T_h^2 + b_2 T_h + b_3 \tag{2}$$
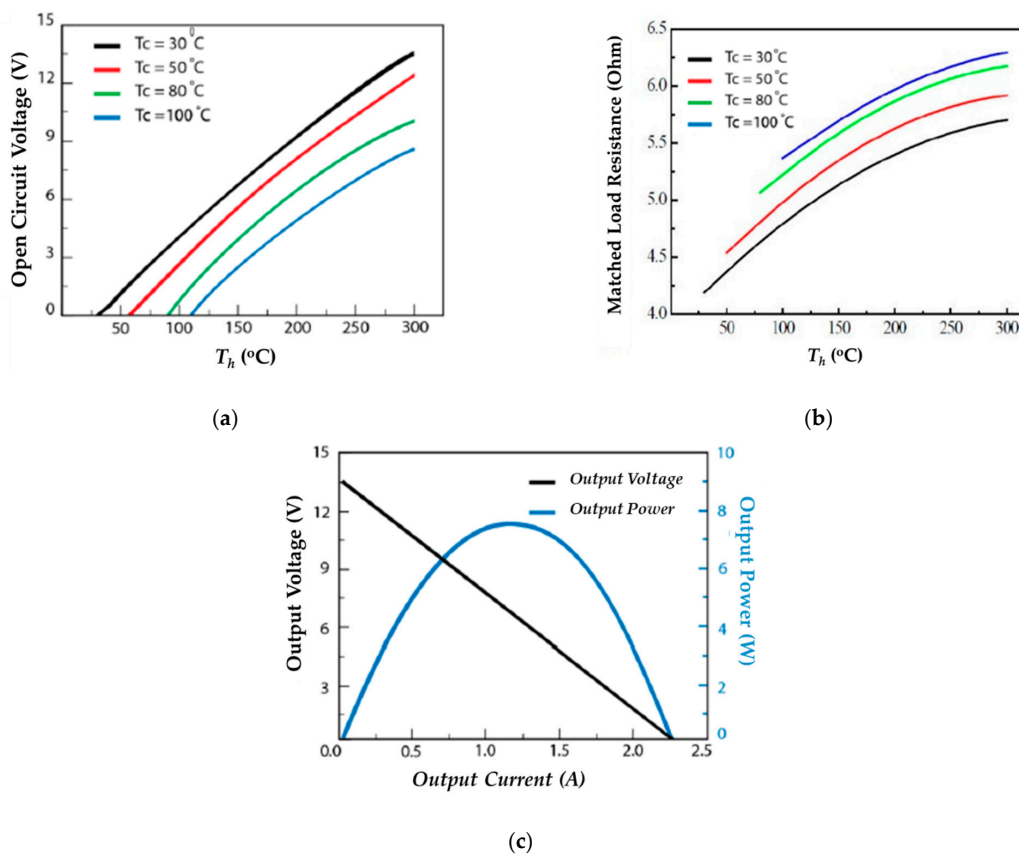

(**a**)

(**b**)

(**c**)

Figure 4. TEM manufacturer datasheet: (**a**) open circuit voltage vs. T_h under various T_c, (**b**) matched load resistance vs. T_h under various T_c, and (**c**) output power and output voltage vs. current under T_h = 300 °C and T_c = 30 °C.

The coefficients a_1, a_2, a_3, b_1, b_2, and b_3 depend on the cold side temperature and are presented in Table 1. From the TEM surface temperatures of the cold and hot side, the open circuit voltage and the internal resistance were obtained.

Table 1. Polynomial coefficients of V_{oc} and R_{int}.

	$V_{oc}=a_1T_h{}^2+a_2T_h+a_3$			$R_{int}=b_1T_h{}^2+b_2T_h+b_3$		
$\mathbf{T_{cold}}$ (°C)	a_1	a_2	a_3	b_1	b_2	b_3
30	-3.994×10^{-5}	6.364×10^{-2}	-1.913	-2×10^{-5}	1.06×10^{-2}	3.886
50	-6.057×10^{-5}	7.218×10^{-2}	-3.925	-2×10^{-5}	1.15×10^{-2}	4.0053
80	-1.052×10^{-4}	8.819×10^{-2}	-6.962	-2×10^{-5}	1.11×10^{-2}	4.2755
100	-8.483×10^{-5}	7.907×10^{-2}	-7.509	-1×10^{-5}	1.05×10^{-2}	4.4514

2.2.2. TEG Electrical Model

A thermoelectric module can be electrically modeled as a voltage source (V_{oc}) connected in series to an internal resistance (R_{int}) [32,33], as Figure 5 shows inside the rectangle with dashed lines.
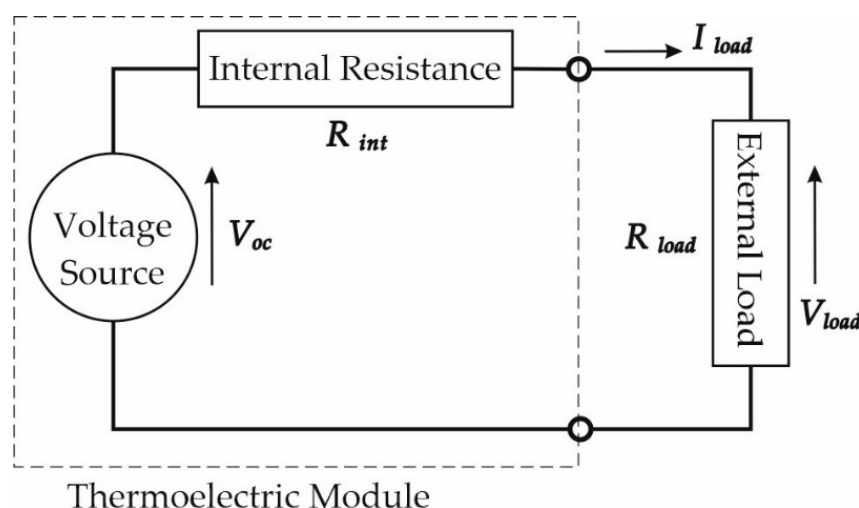

Figure 5. Electrical model of thermoelectric module.

The electrical model of a TEM connected to an external load (R_{load}) can be mathematically written from Equation (3). The electrical current in the circuit is inversely proportional to the sum of the external load and the internal resistance of the TEM, as Equation (4) describes.

$$V_{load} = V_{oc} - R_{int}.I_{load} \tag{3}$$

$$I_{load} = \frac{V_{oc}}{R_{load} + R_{int}} \tag{4}$$

$$P_{load} = I_{load}^2.R_{load} \tag{5}$$

It has been demonstrated, theoretically and experimentally, that the point of maximum power occurs when the external load voltage is equal to half of the voltage value under open circuit [32]. It is possible to connect the TEMs in series, parallel, or in a mixed way (Figure 6) according to the needs of the external load connected to the TEG.
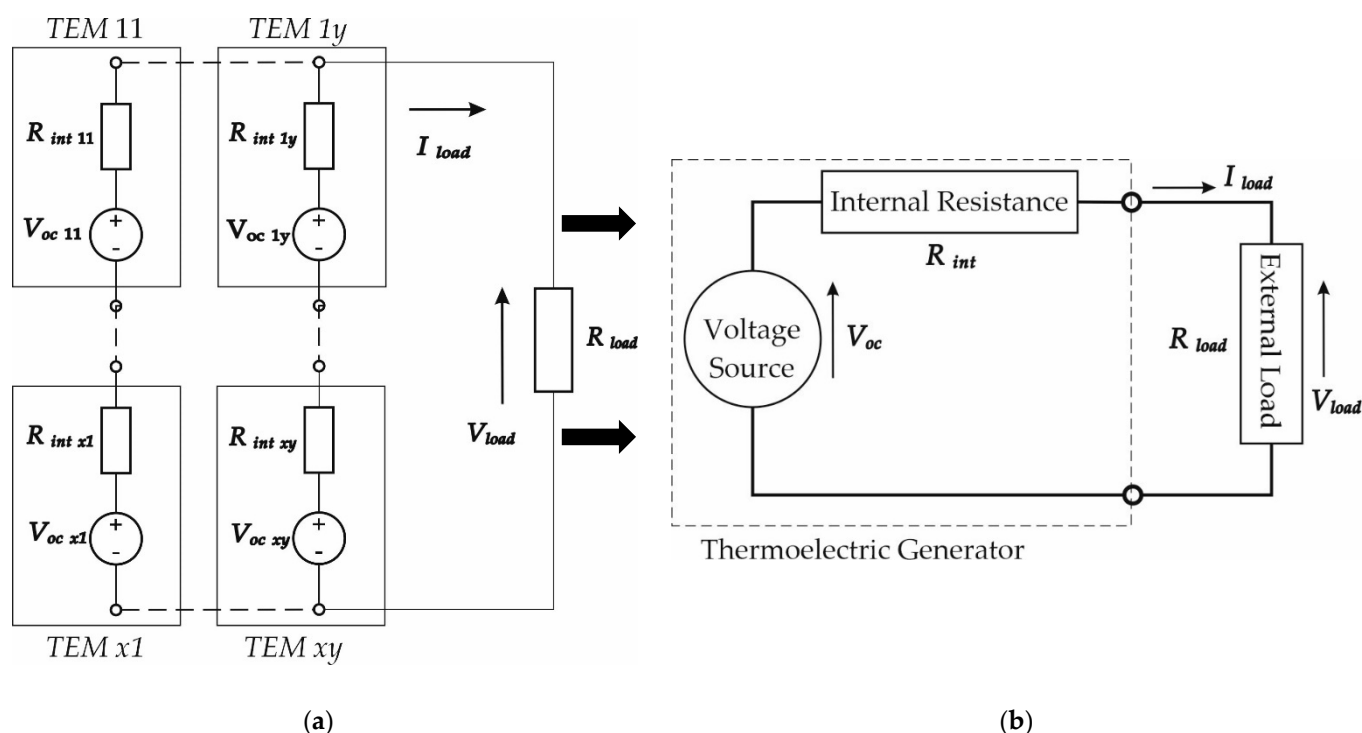
Figure 6. Electrical model diagram of TEMs: (**a**) in series–parallel configuration under heterogeneous thermal surface conditions and (**b**) its equivalent circuit.

Applying both the Kirchhoff law and the Thevenin theorem, it is possible to calculate V_{oc} and R_{int} of the whole thermoelectric generator according to the electrical parameters of the thermoelectric modules following the Equations (6) and (7).

$$V_{oc} = \left(\sum_{j=1}^{y} \frac{\sum_{i=1}^{x} V_{oc_{ij}}}{\sum_{i=1}^{x} R_{int_{ij}}} \right) \cdot \left(\sum_{j=1}^{y} \frac{1}{\sum_{i=1}^{x} R_{int_{ij}}} \right)^{-1} \qquad (6)$$

$$R_{int} = \left(\sum_{j=1}^{y} \frac{1}{\sum_{i=1}^{x} R_{int_{ij}}} \right)^{-1} \qquad (7)$$

3. Experimental Setup

3.1. Experimental Installation

Figure 7 shows a general view of the installation used for the experimental validation of the TEG electrical model presented in the previous section. As the figure shows, the TEG was installed along the exhaust pipe downstream of the diesel oxidation catalyst (DOC) and upstream of the muffler. The reason for this was to avoid the negative influence on the operation of this post-treatment device and to take advantage of the full exergy potential of the exhaust gases.

In this figure, the DOC is located at the hidden side of the picture. The exhaust duct, connecting the DOC to the TEG, was thermally insulated to provide the highest possible thermal energy at the TEG inlet.
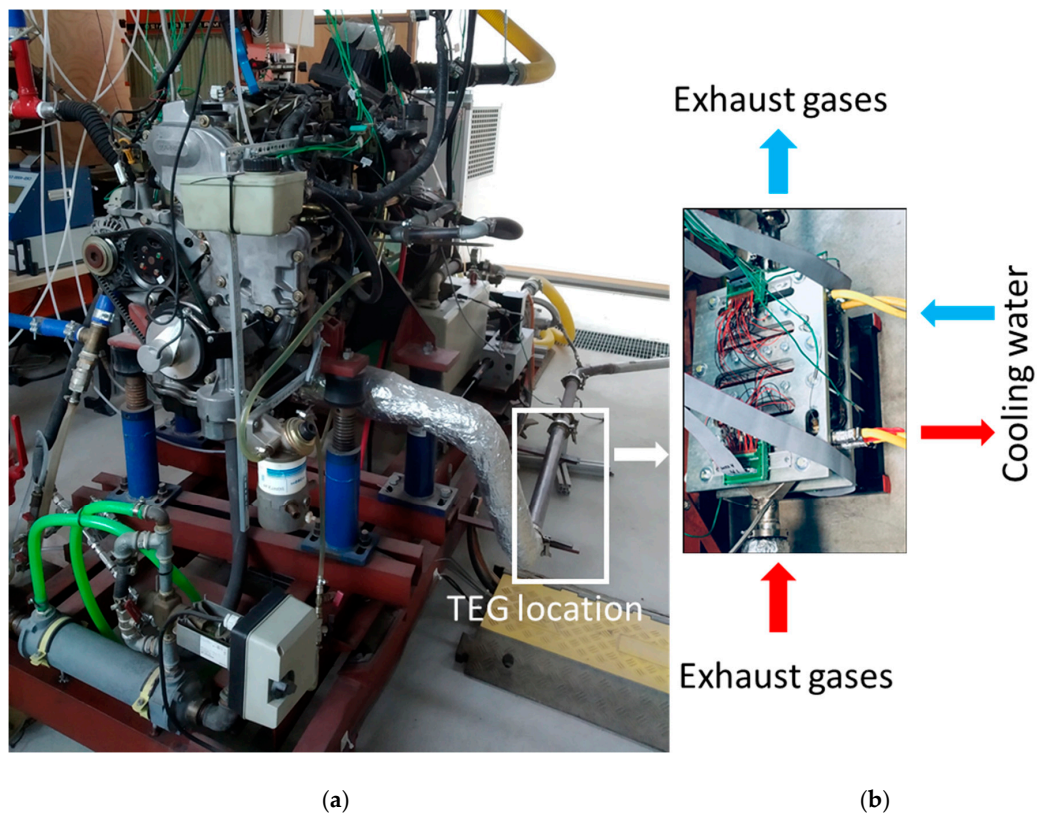
(**a**)   (**b**)

Figure 7. (**a**) Engine test bench and (**b**) the thermoelectric generator coupled to the exhaust pipe.

As the source for thermal energy, a Euro 3 Diesel engine was used. The main characteristics of the engine are presented in Table 2. This engine does not have particulate matter trap nor selective catalytic reactor (SCR), but counts with a DOC. In any case, it is recommendable to install the TEG always downstream of the post-treatment devices to avoid disturbance on their light-off processes.

Table 2. Tested engine.

Engine Type and Model	Diesel, NISSAN YD22
Pollutant standard	Euro 3
Maximum effective power (kW)	82 kW (at 4000 min^{-1})
Maximum effective torque (Nm)	248 Nm (at 2000 min^{-1})
Number of cylinders	4, in line
Cylinder diameter (mm)	86.5
Stroke (mm)	94
Displaced volume (L)	2.2
Compression ratio	16.7
Injection system	High pressure with common rail
Fuel injection pressures	200 bar at ralentí (750 min^{-1}) 1600 bar at max power (4000 min^{-1})
EGR system	External, high pressure and hot
Maximum EGR rate (%)	Up to 25
Supercharging system	Turbocharger regulated with waste gate and including intercooler

3.2. Thermoelectric Generator

Thermoelectric generators used in vehicles are usually located in the exhaust system to take advantage of the residual heat carried by the exhaust gases (heat source) and the cooling water of the engine or the air (heat sink). They are essentially made up of three elements: (i) a heat exchanger in contact with the exhaust gases, (ii) thermoelectric modules that take advantage of the temperature gradient between their two faces to convert thermal energy into electrical energy, and (iii) a water-cooling circuit.

The TEG tested in this work (see Figure 7b), which adopts this same configuration, houses in its central part and along its entire length the modified section of the exhaust pipe (shown in Figure 8a). On the two faces of said modified section, 80 commercial thermoelectric modules of bismuth telluride (Bi_2Te_3) are placed, 40 on each face (Figure 8b). The cold sides of the thermoelectric modules are cooled with two water heat exchangers, one for each side of the TEG. In this work, following the trend in more recent studies [17,18,34,35], the water temperature was set to 50 °C, as this is a realistic temperature that could be achieved with external convection and no extra energy cost.
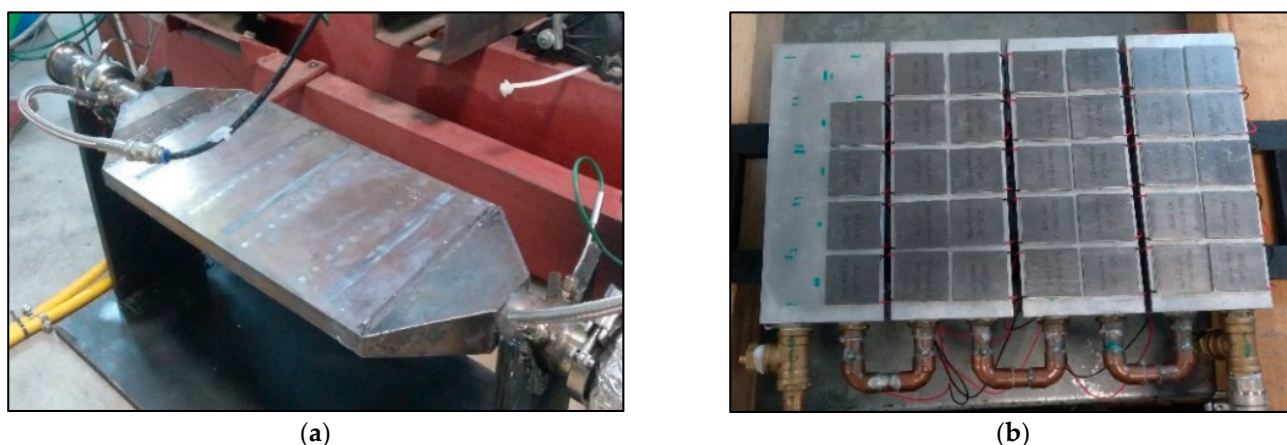

(**a**)

(**b**)

Figure 8. Modified section of the exhaust pipe (**a**) and locations of 40 TEMs on each face (**b**).

As heat is removed from the exhaust gases, the temperature of the exhaust gases decreases along the direction of the flow. This implies that TEMs from the same TEG operate under different hot side temperatures depending on their location. In other words, the temperature of each of the 80 modules of the TEG will be different and, therefore, its electrical output as well. This thermal mismatch causes uneven operation of the TEMs connected on the same branch. Furthermore, the way the TEMs are electrically connected to each other greatly affects the power output of the entire TEG system.

For this reason, since there is still no prediction model for the thermoelectric behavior of the TEMs, it is important to electrically characterize each of the thermoelectric modules. Figure 9 shows an example of the qualitative results of the electrical characterization at half engine load (2400 rpm, 110 Nm). TEMs are colored from red to blue, i.e., from hottest to coldest. Obviously, the direction of the exhaust gas flow is from left to right.

These results reveal a temperature distribution pattern throughout the TEG. To limit the negative effect of thermal mismatch on power generation, TEMs were classified by temperature proximity into four different groups with modules connected in series, as shown in the diagram in Figure 9b.
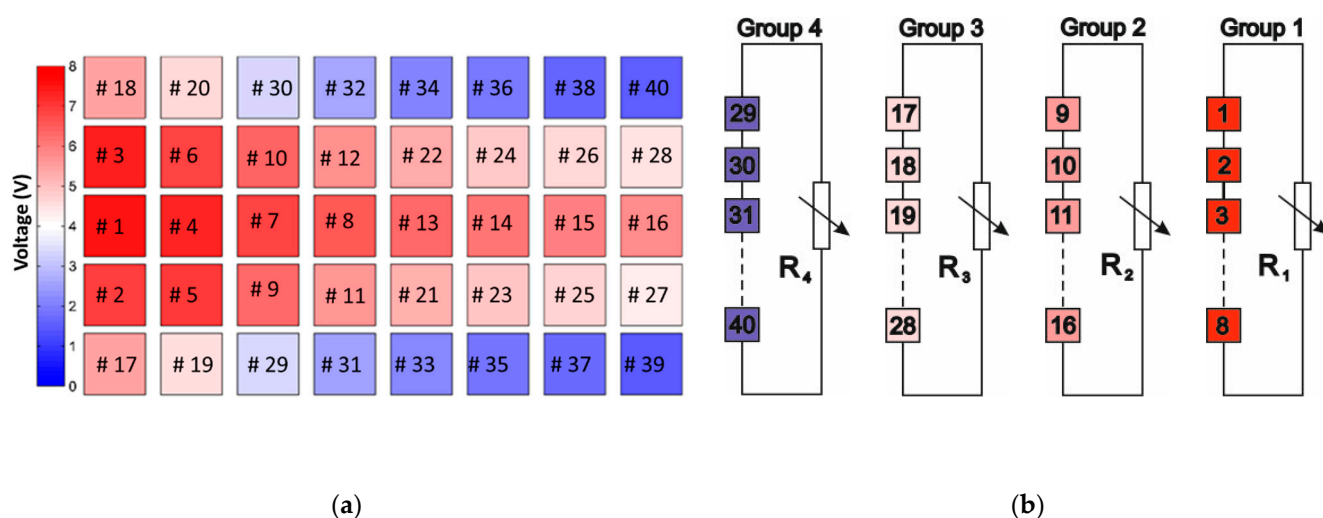
(**a**)　　　　　　　　　　　　　　　　　　　　　　　　　　　　　　(**b**)

Figure 9. (**a**) Thermoelectric modules are numbered (#1–#40) from hotter to colder and (**b**) diagram of the electrical connection of the TEG modules used in this work.

3.3. Test Plan

The test plan was defined in correspondence with the following circumstances:

- The engine used in this work is equipped in different vehicle models which have been homologated according to the past New European Driving Cycle (NEDC) normative.
- Nowadays light-duty vehicles must be homologated following the new World-wide Harmonized Light-Duty Vehicles Test Procedures (WLTP).
- Both effective torque and power of the brake used in the test bench were limited.
- Previous results were published in the following references [7,31,36,37].

The test plan was according to the engine operating modes selected and using the longitudinal dynamic equations of a vehicle [38]. By means of the data of the vehicle speed profile and the gearbox position each instant of the NEDC, each vehicle operation point was translated to the respective engine operation mode.

According to these results, a great number of steady-state engine modes was obtained, which are presented on the effective torque–engine speed map (Figure 10b). In black, those modes translated from the NEDC and, in grey, those translated from the WLTP (Figure 10a) are presented.
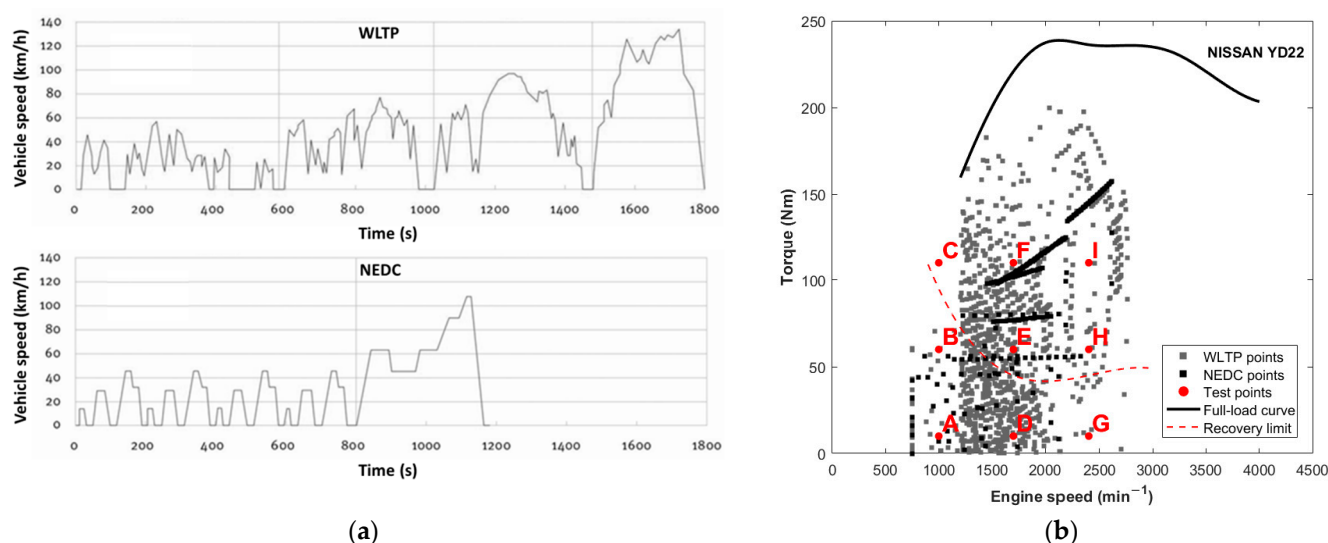

(**a**)　　　　　　　　　　　　　　　　　　　　　　　　　　　　　　(**b**)

Figure 10. (**a**) Examples of the vehicle speed profiles under WLTP and NEDC certification cycles and (**b**) steady state operating modes translated by means of longitudinal dynamic equations for a vehicle.

The obtained results gave us the possibility to define some steady-state test modes, located on that part of the engine torque–engine speed map, with representativeness of both the urban and extra-urban driving. The modes selected were determined according to a previous work of experiment design [39].

In Table 3, torque and engine speed of the engine modes tested are shown. Nomenclature A, B, C, D, E, F, G, H, and I also correspond to the test plans with objectives of other works [40,41]. These modes are presented in Figure 10b with red dots.

Table 3. Engine performance (torque and engine speed) in tested operating modes.

n, Engine Speed (min^{-1})	Me, Effective Torque (Nm)		
	10	60	110
1000	A	B	C
1700	D	E	F
2400	G	H	I

As can be seen in Figure 10b, the operating modes chosen on the effective torque–engine speed map mainly cover the lower left quadrant of this map. These points are mainly located in the zone of the engine map which characterizes the urban driving of the vehicle.

4. Result and Discussion

4.1. Model Validation

To evaluate the TEG electrical model, the chosen engine operating modes lie on the part of the torque–engine speed map commonly used under urban driving, as can be seen in Figure 10a. The model presented in this work (see Table 4) has been validated by comparison of the measured and calculated parameters by the model under the same operating conditions.

Table 4. Experimental values vs. theoretical values.

Engine Operating Mode		A	G	E	H	C	F	I
Electrical output power (W)	Measured	0.30	3.40	10.20	25.80	15.70	31.70	56.70
	Calculated	0.35	3.94	11.78	27.02	16.56	32.77	58.20
Relative error (%)		16.67	15.88	15.49	4.73	5.48	3.38	2.65
RMSE (W)					1.10			

As can be seen in Table 4, the relative error between the calculated and measured values is smaller as the engine load increases. This means that the model is more accurate in engine operating modes where the TEG generates more electrical energy, since the relative proportion of electrical energy losses becomes lower.

4.2. Simulated Scenarios

Results were obtained by simulation of three possible scenarios: (i) thermal mismatch among thermoelectric modules in the same electrical branch, (ii) malfunction of some modules, and (iii) variation of the number of modules in a branch.

4.2.1. Scenario 1

Figure 11 shows the different groups of TEMs studied. In this scenario, the obtained electrical energy produced by each group of TEMs interconnected between them is compared to the sum of the electric energy generated by each TEM of each group but electrically disconnected between them. The objective of this comparison was to assess the effect of

TEM connection under different cases of different thermal conditions (due to the position of the TEMs in respect to the hot surface and the operating mode of the engine).
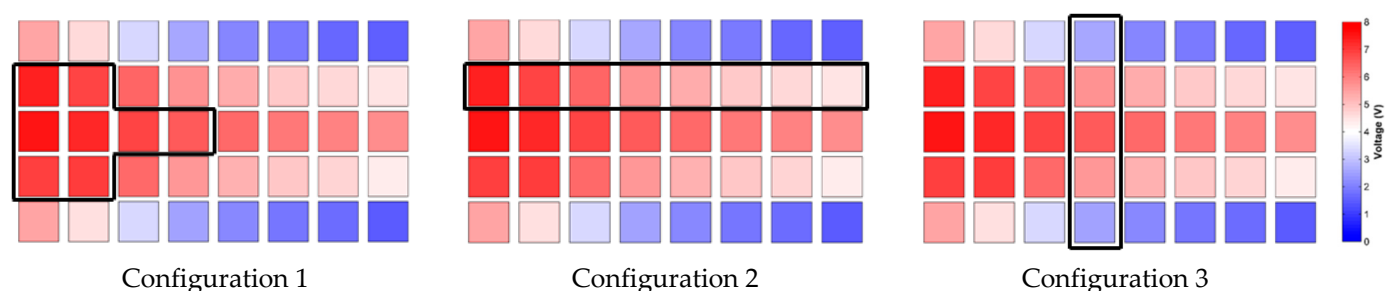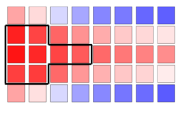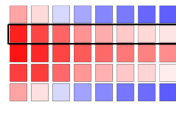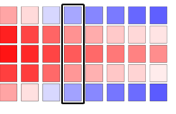

Figure 11. Connection configurations of different groups of TEMs.

Table 5 shows the results of the calculation of the difference in electrical energy produced, comparing the different connection configurations presented in Figure 10. The results are shown for the three modes with the highest production of the thermoelectric generator (Modes F, I and H, see Figure 10b).

Table 5. Relative differences of the electric energy losses from each configuration presented in Figure 11 and under three of the engine operating modes.

Mode	Me (Nm)	n (min^{-1})	Relative Differences of the Electric Power Produced by Each Configuration Comparing Two Situations: Energy Produced by the Interconnected TEMs vs. the Sum of the Energy Produced by These TEMs Disconnected between Them (%)		
			Configuration 1	Configuration 2	Configuration 3
I	110	2400	−0.27	−3.17	−8.97
F	110	1700	−0.44	−5.01	−12.18
H	60	2400	−0.71	−7.57	−17.55

Considering the results obtained in mode I and each of the studied configurations, it is possible to observe that the electrical connection of the TEMs, under thermal mismatch conditions, has a negative effect on the production of electrical energy of the TEMs together (all TEMs are electrically connected to the same load) compared to the sum of the energies generated by each of these same TEMs when they are electrically disconnected from each other (individually controlled). The greater the difference in the temperature of the hot surface to which each TEM is exposed, the lower the energy produced by the interconnected set with respect to the same TEMs but disconnected from each other.

This thermal mismatch is generated, mainly for two reasons:

- The temperature of the exhaust gases decreases along the flow direction as the heat is transmitted from the gas to the duct wall;
- The distribution of the gas flow inside the exchanger section where the TEMs are placed.

This assumes that TEMs operate under substantially different hot side temperatures depending on their location.

However, there are two other possible reasons that motivate a decrease in electrical energy production due to superficial thermal differences:

- The variability of the electrothermal performance of the TEMs;
- The mechanical clamping pressure of each TEM.

4.2.2. Scenario 2

Inadequate mounting pressure for TEMs, continuous operation under extreme thermal conditions, or the presence of manufacturing defects are sufficient causes for a TEM to stop working properly.

This second scenario simulates the situation in which a TEM malfunctions and stops producing electrical power. However, its internal resistance continues to consume energy, due to the Joule effect. In this case, the energy loss due to the malfunction of a single thermoelectric module, as presented in Figure 12, is very important, compared to the case where all the TEMs work correctly. Hence, there is a need to incorporate protective electronic components, for example, bypass diodes, to prevent the passage of electric current through faulty TEMs to prevent them from becoming electrical charges. The result showing a reduction of 24% in the electrical energy produced has been obtained for configuration 1 and in operating mode I.
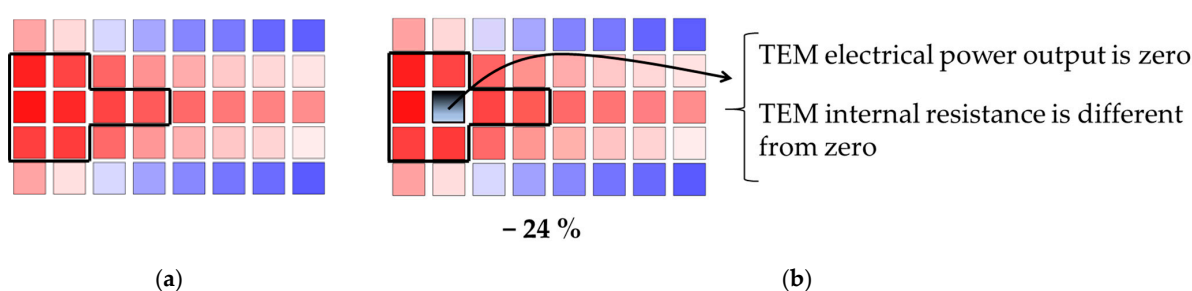

Figure 12. Connection configurations of different groups of TEMs.

4.2.3. Scenario 3

The third scenario tries to determine the most suitable electrical configuration for the TEG tested in terms of the number of TEMs for each electrical branch. There are several options that go from connecting in series all the TEMs of the TEG to the option in which each of the TEMs is controlled individually.

In Figure 13, three possible situations are exemplified:

a.　All the TEMs available in the TEG are electrically connected in series.

b.　Two groups of TEMs are constituted whose temperatures are as homogeneous as possible and each group is connected (separately) to its adjusted electrical load to achieve the maximum electrical power.

c.　Four groups of TEMs are constituted with temperatures as homogeneous as possible among them and each group is connected (separately) to its adjusted electrical load to achieve the maximum electrical power.

d.　Then, the electrical power generated in options b) and c) are compared with the electrical power achieved by the TEG in the configuration of option a) to verify the degree of improvement in the performance of the TEG.
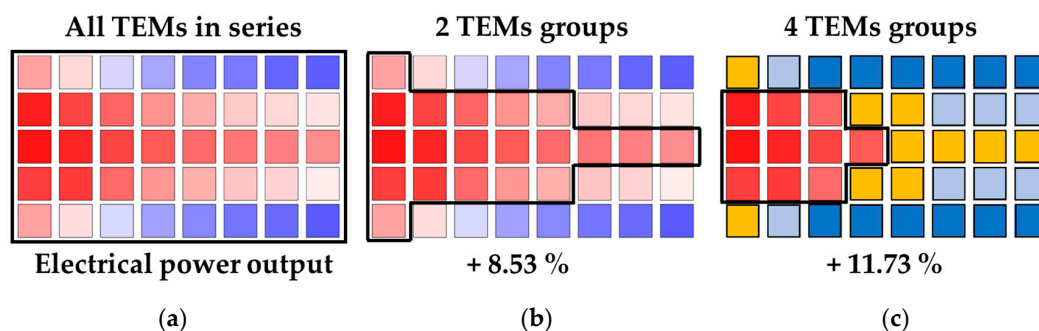

Figure 13. Comparison of the electric energy generated by the TEG depending on the connection of the TEMs: (**a**) all TEMs in series, (**b**) 2 TEM groups, and (**c**) 4 TEM groups.

According to the results provided in Figure 13, the greater the number of groups of interconnected TEMs and the lower the number of TEMs in each electrical branch, the greater the electrical energy recovered by the TEG. For two groups of TEMs, an increase in electrical energy produced of more than 8% is calculated, while for four groups, an increase of almost 12% is calculated. However, these improvements make the control circuit more complicated and expensive due to the increase in the number of converters required. The most suitable configuration for this type of TEG is to find a balance between the number of converters and the number of TEMs connected to each converter. This will be the main objective of the next research work of the authors of this study.

5. Conclusions

In this work, a simple but effective model has been developed. The model can predict the electrical behavior of a thermoelectric generator when its electrically interconnected modules are exposed to non-uniform hot surfaces.

Before connecting the TEMs electrically, it is important to characterize each one of the modules individually to detect temperature mismatches between the TEMs or malfunction of any of them.

The simulation of several scenarios allows to state that: (i) the power lost by mismatched conditions can be very significant, (ii) it is necessary to protect the electrical circuit against the malfunction of some TEMs, and (iii) a balance must be found between the number of MPPT converters and the number of TEG modules connected to each converter.

The results show that the electrical interconnection between modules will depend on a problem to be solved before: the uniformity of the temperature to which the hot face of the interconnected modules is exposed in the generator.

References

1. Ezzitouni, S.; Fernández-Yáñez, P.; Sánchez, L.; Armas, O. Global energy balance in a diesel engine with a thermoelectric generator. *Appl. Energy* **2020**, *269*, 115139. [CrossRef]
2. Payri, F.; Olmeda, P.; Martín, J.; Carreño, R. Experimental analysis of the global energy balance in a DI diesel engine. *Appl. Therm. Eng.* **2015**, *89*, 545–557. [CrossRef]
3. Torregrosa, A.J.; Olmeda, P.C.; Martín, J.; Romero, C.A. A tool for predicting the thermal performance of a diesel engine. *Heat Transf. Eng.* **2011**, *32*, 891–904. [CrossRef]
4. Caputo, S.; Millo, F.; Boccardo, G.; Piano, A.; Cifali, G.; Concetto, F. Numerical and experimental investigation of a piston thermal barrier coating for an automotive diesel engine application. *Appl. Therm. Eng.* **2019**, *162*, 114233. [CrossRef]
5. Wang, Y.; Ma, T.; Liu, L.; Yao, M. Numerical investigation of the effect of thermal barrier coating on combustion and emissions in a diesel engine. *Appl. Therm. Eng.* **2021**, *186*, 116497. [CrossRef]
6. García-Contreras, R.; Soriano, J.A.; Fernández-Yáñez, P.; Sánchez, L.; Mata, C.; Gómez, A.; Armas, O.; Cárdenas, M.D. Impact of regulated pollutant emissions of Euro 6d-Temp light-duty diesel vehicles under real driving conditions. *J. Clean. Prod.* **2021**, *286*, 124927. [CrossRef]

7. Fernández-Yañez, P.; Armas, O.; Kiwan, R.; Stefanopoulou, A.G.; Boehman, A.L. A thermoelectric generator in exhaust systems of spark-ignition and compression-ignition engines. A comparison with an electric turbo-generator. *Appl. Energy* **2018**, *229*, 80–87. [CrossRef]

8. Arsie, I.; Cricchio, A.; Pianese, C.; Ricciardi, V.; De Cesare, M. Modeling Analysis of Waste Heat Recovery via Thermo-Electric Generator and Electric Turbo-Compound for CO2 Reduction in Automotive SI Engines. *Energy Procedia* **2015**, *82*, 81–88. [CrossRef]

9. Comamala, M.; Pujol, T.; Cózar, I.R.; Massaguer, E.; Massaguer, A. Power and fuel economy of a radial automotive thermoelectric generator: Experimental and numerical studies. *Energies* **2018**, *11*, 2720. [CrossRef]

10. Iniesta, C.; Olazagoitia, J.L.; Vinolas, J.; Gros, J. New method to analyse and optimise thermoacoustic power generators for the recovery of residual Energy. *Alex. Eng. J.* **2020**, *59*, 3907–3917. [CrossRef]

11. Wachter, P.; Gaber, C.; Demuth, M.; Hochenauer, C. Towards a recuperative, stationary operated thermochemical reformer: Experimental investigations on the methane conversion and waste heat recovery. *Appl. Therm. Eng.* **2021**, *183*, 116121. [CrossRef]

12. Di Battista, D.; Fatigati, F.; Carapellucci, R.; Cipollone, R. An improvement to waste heat recovery in internal combustion engines via combined technologies. *Energy Convers. Manag.* **2021**, *232*, 113880. [CrossRef]

13. Jaziri, N.; Boughamoura, A.; Müller, J.; Mezghani, B.; Tounsi, F.; Ismail, M. A comprehensive review of Thermoelectric Generators: Technologies and common applications. *Energy Rep.* **2019**, *6*, 264–287. [CrossRef]

14. Anatolyevich, K.; Yurievich, L.L.; Pavlovich, T.A.; Viktorovich, S.R.; Alekseyevich, S.A. Turbo- Generators in Energy Recovery Systems. *Int. J. Res. Mech. Eng. Technol.* **2018**, *9*, 1009–1018.

15. Raghulnath, D.; Saravanan, K.; Mahendran, J.; Ranjith Kumar, M.; Lakshmanan, P. Analysis and optimization of organic Rankine cycle for IC engine waste heat recovery system. *Mater. Today* **2020**, *21*, 30–35. [CrossRef]

16. Yue, C.; Tong, L.; Zhang, S. Thermal and economic analysis on vehicle energy supplying system based on waste heat recovery organic Rankine cycle. *Appl. Energy* **2019**, *248*, 241–255. [CrossRef]

17. Mori, M.; Yamagami, T.; Sorazawa, M.; Miyabe, T. Simulation of fuel economy effectiveness of exhaust heat recovery system using thermoelectric generator in a series hybrid. *SAE Int. J. Mater. Manuf.* **2011**, *4*, 1268–1276. [CrossRef]

18. Li, X.; Xie, C.; Quan, S.; Shi, Y.; Tang, A.Z. Optimization of thermoelectric modules' number and distribution pattern in an automotive exhaust thermoelectric generator. *IEEE Access* **2019**, *7*, 72143–72157. [CrossRef]

19. Shu, G.; Ma, X.; Tian, H.; Yang, H.; Chen, T.; Li, X. Configuration optimization of the segmented modules in an exhaust-based thermoelectric generator for engine waste heat recovery. *Energy* **2018**, *160*, 612–624. [CrossRef]

20. LaGrandeur, J.; Crane, D.; Hung, S.; Mazar, B.; Eder, A. Automotive waste heat conversion to electric power using skutterudite, TAGS, PbTe and BiTe. In Proceedings of the 25th International Conference on Thermoelectrics, Vienna, Austria, 6–10 August 2006; pp. 343–348. [CrossRef]

21. Hussain, Q.; Brigham, D.; Maranville, C. Thermoelectric exhaust heat recovery for hybrid vehicles. *SAE Int. J. Eng.* **2009**, *2*, 1132–1142. [CrossRef]

22. Meng, F.; Chen, L.; Sun, F. A numerical model and comparative investigation of a thermoelectric generator with multi-irreversibilities. *Energy* **2011**, *36*, 3513–3522. [CrossRef]

23. Xiaolong, G.; Suwen, Y.; Heng, X.; Qiang, O. A dynamic model for thermoelectric generator applied in waste heat recovery. *Energy* **2013**, *52*, 201–209. [CrossRef]

24. Kumar, S.; Heister, S.D.; Xu, X.; Salvador, J.R.; Meisner, G.P. Thermoelectric generators for automotive waste heat recovery systems part I: Numerical modeling and baseline model analysis. *J. Electron. Mater.* **2013**, *42*, 665–674. [CrossRef]

25. Hsiao, Y.Y.; Chang, W.C.; Chen, S.L. A mathematic model of thermoelectric module with applications on waste heat recovery from automobile engine. *Energy* **2010**, *35*, 1447–1454. [CrossRef]

26. Massaguer, E.; Massaguer, A.; Pujol, T.; Gonzalez, J.R.; Montoro, L. Modelling and analysis of longitudinal thermoelectric energy harvesters considering series-parallel interconnection effect. *Energy* **2017**, *129*, 59–69. [CrossRef]

27. Comamala, M.; Cózar, I.R.; Massaguer, A.; Massaguer, E.; Pujol, T. Effects of Design Parameters on Fuel Economy and Output Power in an Automotive Thermoelectric Generator. *Energies* **2018**, *11*, 3274. [CrossRef]

28. Torrecilla, M.C.; Montecucco, A.; Siviter, J.; Knox, A.R.; Strain, A. Novel model and maximum power tracking algorithm for thermoelectric generators operated under constant heat flux. *Appl. Energy* **2019**, *256*, 113930. [CrossRef]

29. Cózar, I.R.; Pujol, P.; Lechocky, M. Numerical analysis of the effects of electrical thermal configurations of thermoelectric modules in large-scale thermoelectric generators. *Appl. Energy* **2018**, *229*, 264–280. [CrossRef]

30. Montecucco, A.; Siviter, J.; Knox, R. The effect of temperature mismatch on thermoelectric generators electrically connected in series and parallel. *Appl. Energy* **2014**, *123*, 47–54. [CrossRef]

31. Fernández-Yañez, P.; Armas, O.; Capetillo, A.; Martínez-Martínez, S. Thermal analysis of a thermoelectric generator for light-duty diesel engines. *Appl. Energy* **2018**, *226*, 690–702. [CrossRef]

32. Rowe, D.; Min, G. Evaluation of thermoelectric modules for power generation. *J. Power Sources* **1998**, *73*, 193–198. [CrossRef]

33. Lineykin, S.; Ben-Yaakov, S. Modeling and analysis of thermoelectric modules. *IEEE Trans. Ind. Appl.* **2007**, *43*, 505–512. [CrossRef]

34. Massaguer, A.; Massaguer, E.; Comamala, M.; Pujol, T.; Montoro, L.; Cardenas, M.D. Transient behavior under a normalized driving cycle of an automotive thermoelectric generator. *Appl. Energy* **2017**, *206*, 1282–1296. [CrossRef]

35. Crane, D.; Lagrandeur, J.; Jovovic, V.; Ranalli, M.; Adldinger, M.; Poliquin, E. TEG on vehicle performance and model validation and what it means for further TEG development. *J. Electron. Mater.* **2013**, *42*, 1582. [CrossRef]

36. Ezzitouni, S.; Fernández-Yáñez, P.; Sánchez, L.; Armas, O.; Soto, F. Effect of the use of a thermoelectric generator on the pumping work of a Diesel engine. *Int. J. Engine Res.* **2019**, 1–12. [CrossRef]
37. Fernandez-Yañez, P.; Gómez, A.; García-Contreras, R.; Armas, O. Evaluating thermoelectric modules in diesel exhaust systems: Potential under urban and extra-urban driving conditions. *J. Clean. Prod.* **2018**, *182*, 1070–1079. [CrossRef]
38. Pacejka, H.B. *Tire and Vehicle Dynamics*, 3rd ed.; Elsevier Ltd.: Amsterdam, The Netherlands, 2012.
39. Torres-Jiménez, E.; Armas, O.; Lešnik, L. Methodology to simulate normalized testing cycles for engines and vehicles via design of experiments with low number of runs. *Energy Convers. Manag.* **2018**, *177*, 817–832. [CrossRef]
40. Soriano, J.A.; Mata, C.; Armas, O. A zero-dimensional model to simulate injection rate from first generation common rail diesel injectors under thermodynamic diagnosis. *Energy* **2018**, *158*, 845–858. [CrossRef]
41. Fernández-Yáñez, P.; Armas, O.; Gómez, A. Developing Computational Fluid Dynamics (CFD) Models to Evaluate Available Energy in Exhaust Systems of Diesel Light-Duty Vehicles. *Appl. Sci.* **2017**, *7*, 590. [CrossRef]